Observation of zeros and amplification of quadrupole-matrix-element contributions to photoelectron angular distributions

M. S. Wang, Young Soon Kim,* R. H. Pratt, and Akiva Ron[†]
Department of Physics and Astronomy, University of Pittsburgh, Pittsburgh, Pennsylvania 15260
(Received 28 September 1981)

We point out several possible observable features of quadrupole contributions to intermediate- and low-energy photoelectron angular distributions $d\sigma/d\Omega$, including zeros (Cooper minima) in the quadrupole-matrix elements. These features result in deviations from the dipole symmetry of $d\sigma/d\Omega$ about 90° (under $\theta\rightarrow\pi-\theta$) and include an oscillation with energy in distributions which vary from peaking forward and backward of 90°. The quadrupole contribution to photoelectron angular distributions can remain significant even for outer shells in the low-energy region, particularly when there are zeros (Cooper minima) in the dominant dipole-matrix elements. As an example we discuss the photoelectron angular distribution from the 5s subshell of tin and estimate the magnitudes of the deviations from symmetry which would be the experimental signatures of these features.

In this paper we discuss the role of quadrupole-matrix elements in determining the character of low- and intermediate-energy photoelectron angular distributions. Recent theoretical work[1-6] has considered the effect of correlations between atomic electrons and the effect of relativity on low-energy outer-shell photoelectron angular distributions, but within the electric dipole approximation. In contrast, Tsěng *et al.*[7] found that higher multipole contributions are important in determining the features of the angular distribution for inner shells of high-Z elements, even for photon energies down to the K- or L-shell threshold.

Here we want to point out that in some circumstances the quadrupole contributions can have a significant effect on the character of photoelectron angular distributions for outer shells in the low- and intermediate-photoelectron-energy region. We describe these features in terms of the general relativistic multipole angular distribution[8]

$$\frac{d\sigma}{d\Omega}=\frac{\sigma_{nLJ}}{4\pi}\sum_{m}B_m P_m(\cos\theta)\ ,$$

where $B_0=1$ and the angular distribution coefficients B_m can be expressed in terms of multipole radial matrix elements and continuum electron phase shifts. B_1 and B_3 vanish in dipole approximation; at low energy they can be specified in terms of products of dipole- and quadrupole-matrix elements and differences of p- and d-wave phase shifts (see below). The contribution of the quadrupole-matrix elements can be seen in the following features of the angular distribution:

(1) B_1 and B_3 can be enhanced in the region of zeros (Cooper minima) of dipole-matrix elements, where the relative magnitude of the quadrupole-matrix elements increases.

(2) The quadrupole-matrix elements themselves have zeros (exhibit the Cooper minimum phenomena), which can cause sign changes in B_1 and B_3.

These observable magnitudes and features of B_1 and B_3, which are due to the quadrupole-matrix elements, result in deviations from the dipole symmetry of $d\sigma/d\Omega$ about 90° (under $\theta\rightarrow\pi-\theta$) including oscillation with energy in distributions peaking forward and backward of 90°.

As an example we consider predictions for the photoelectron angular distribution from the 5s subshell of tin within a single electron transition Dirac-Slater central potential calculation. In Fig. 1 we show as a function of photoelectron energy T the cross section σ and the first few angular distribution coefficients B_m. The dominant coefficient is B_2 and its dominant feature is the rapid variation near 10 eV associated with the Cooper minima of dominant dipole-matrix elements.[9] We have expanded the scale of the smaller coefficients (B_1,B_3) which are the subject of this paper, so that one can see their sign changes, the approximate symmetry $B_1\sim-B_3$, and the enhancement when B_2 is rapid-

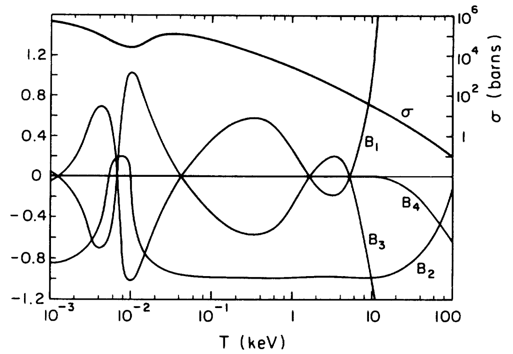

FIG. 1. Photoeffect cross section σ and angular distribution coefficients B_1, B_2, B_3, B_4 for the 5s subshell of tin as a function of photoelectron energy. The right-hand-side scale is for the cross section (barns), the left-hand scale for B's. In plotting the graph, B_1 and B_3 were multiplied by 10.

ly varying.

We wish to understand these coefficients in terms of multipole radial matrix elements, defined as[8]

$$R^{\Lambda\lambda 2jl}_{n2JL} = (-\kappa||S^{\lambda}_{\Lambda}||K)\int G_K j_\lambda f_\kappa dr - (\kappa||S^{\lambda}_{\Lambda}||-K)\int F_K j_\lambda g_\kappa dr \,,$$

where G, F and g,f are the large and small components of Dirac electron wave functions of bound and continuum states, respectively, j_λ is the spherical Bessel function, K and κ are the bound and continuum Dirac quantum numbers, J,L and j,l are initial- and final-state photoelectron total and orbital angular momentum and[8]

$$(\kappa'||S^{\lambda}_{\Lambda}||K') = (-1)^{L'}\left[\frac{3}{8\pi}(2j'+1)(2J'+1)(2\Lambda+1)(2l'+1)(2L'+1)\right]^{1/2} C(l'L'\lambda;00)X\begin{Bmatrix}\lambda & 1 & \Lambda\\ l' & \frac{1}{2} & j'\\ L' & \frac{1}{2} & J'\end{Bmatrix}.$$

For low energies (small k) $j_\lambda(kr)\sim(kr)^\lambda$ where k is the incident photon momentum and the multipole matrix element will be small for higher λ. Also it can be shown that the leading terms of $R^{1110}_{n\,10}$ and $R^{1132}_{n\,10}$ are of order $(E_{nLJ}/m_ec^2)kr$ instead of kr, where E_{nLJ} is the binding energy of the nLJ state (here $L=0$, $J=\frac{1}{2}$). For these reasons, in the low-energy region the leading contributions to an outer s subshell cross section σ and its angular distribution coefficients B_1, B_2, B_3 are

$$\sigma = \frac{8\pi\alpha pE}{9k}[(1011)^2+2(1031)^2]\,, \tag{1a}$$

$$B_1 = \frac{4\pi\alpha pE}{25k\sigma}[5(1011)(2132)\cos(\delta_1-\delta_2)+(1031)(2132)\cos(\delta_{-2}-\delta_2) + 9(1031)(2152)\cos(\delta_{-2}-\delta_{-3})]\,, \tag{1b}$$

$$B_2 = -\frac{8\pi\alpha pE}{9k\sigma}[(1031)^2+2(1031)(1011)\cos(\delta_{-2}-\delta_1)]\,, \tag{1c}$$

$$B_3 = -\frac{4\pi\alpha pE}{25k\sigma}[5(1011)(2152)\cos(\delta_1-\delta_{-3})+6(1031)(2132)\cos(\delta_{-2}-\delta_2) + 4(1031)(2152)\cos(\delta_{-2}-\delta_{-3})]\,, \tag{1d}$$

where[10]

$$(1011)=\sqrt{24\pi}R^{1011}_{n\,10},\quad (1031)=-\sqrt{12\pi}R^{1031}_{n\,10}\,,$$

$$(2132)=\sqrt{40\pi}R^{2132}_{n\,10},\quad (2152)=-\left[\frac{80\pi}{3}\right]^{1/2}R^{2152}_{n\,10}\,,$$

and p, E, and k are photoelectron momentum and energy and photon momentum, $\delta_\kappa-\delta_{\kappa'}$ is the difference between the phase shifts of continuum states of Dirac quantum numbers κ and κ'. In the nonrelativistic limit (1011)=(1031) and corresponds to the nonrelativistic dipole-matrix element, (2132)=(2152) and corresponds to the nonrelativistic quadrupole-matrix element, $\delta_{-2}-\delta_1=0$,

$$\delta_1-\delta_2=\delta_{-2}-\delta_2=\delta_{-2}-\delta_{-3}$$
$$=\delta_1-\delta_{-3}=\delta_p-\delta_d\ ,$$

$B_2=-1$, and $B_1=-B_3$.

In Fig. 2 we show for the 5s subshell of Sn these matrix elements and phase-shift differences as a function of photoelectron energy T. We see that the relative magnitude of the quadrupole terms remains significant down to threshold. When the photoelectron energy is in and below the keV region (less than 10 keV) higher multipole contribution are small compared with these dipole[11] and quadrupole terms. Figure 2 shows that even near the Cooper mimima (zeros) of the dipole-matrix elements the dipole terms still dominate due to their relativistic splitting. So throughout this energy range σ and B_2 are mainly determined by the dipole-matrix elements, B_1 and B_3 by the dipole- and quadrupole-matrix elements and the phase-shift differences, in accord with Eq. (1). The behavior of B_2, including its major structure and deviation from nonrelativistic behavior, associated with the displaced zeros of the two dipole-matrix elements, has been discussed previously.[9] Here we will focus on the behavior of B_1 and B_3, governed by the dipole- and quadrupole-matrix elements and phase-shift differences.

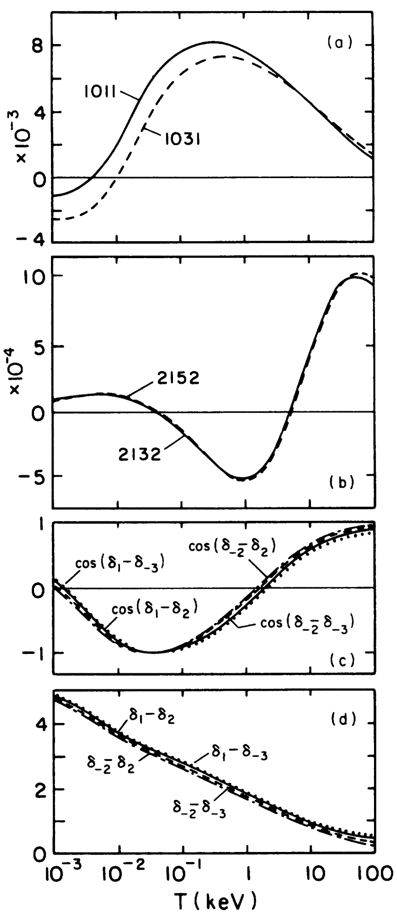

FIG. 2. Results for (a) dipole and (b) quadrupole-matrix elements, for (c) the cosine of phase-shift differences and (d) the phase-shift differences themselves. In (a) solid line —— (1011), dashed line ---- (1031); (b) solid line —— (2132), dashed line ---- (2152); (c) solid line —— $\cos(\delta_1-\delta_2)$, dashed line ---- $\cos(\delta_{-2}-\delta_{-3})$, dotted line $\cdots$ $\cos(\delta_1-\delta_{-3})$, broken line —.—.—.— $\cos(\delta_{-2}-\delta_2)$; (d) same as (c) for the phase-shift differences.

Since the numerator of our expression for B_1 and B_3 is linear in the dipole-matrix elements while the denominator σ is quadratic in them, we expect that in the region where the dipole-matrix elements change sign the values of B_1 and B_3 can be enhanced. This requires that the splitting between the two dipole-matrix elements not be too large, so that a significant Cooper minimum can be observed in the subshell cross section, but also not so small that σ is determined by the quadrupole terms and B_1 and B_3 become linear in still higher multipoles. Further, assuming the quadrupole-matrix elements and phase shifts are slowly varying through the enhancement region, B_1 and B_3 must change sign in the middle of the region of their enhancement, since both dipole elements change sign in the course of this region. Figure 1 illustrates this behavior in our calculation for the 5s subshell of tin, showing an enhancement in B_1 and B_3 associated with the zeros (Cooper minima) of the dipole-matrix elements. (In the uranium 7s subshell[9] the splitting between the two dipole-matrix elements is larger, the Cooper minima do not have a significant effect on the cross section, and there is no significant enhancement of B_1 and B_3, which do still change sign.)

While Fig. 2 shows one sign change for each dipole-matrix element (the well known Cooper minimum), it shows two sign changes for the quadrupole-matrix elements above threshold; there are also two sign changes in the cosine of the phase-shift differences which enter the expressions for B_1 and B_3. (The magnitude for the phase-shift difference near threshold is consistent with Manson's Hartree-Slater calculation.[12]) From these features and the formula [(1b),(1d)] the origin of the five zeros of B_1 and B_3 in Fig. 1 can be identified. These zeros, in order from high energy to low energy, are due (1) to the first sign change of the quadrupole-matrix element, (2) to the first sign change of the cosine of the phase difference, (3) to the second sign change of the quadrupole-matrix element, (4) to the sign change of the dipole-matrix element (normal Cooper minimum), and (5) to the second sign change in the cosine of the phase difference. To the extent that the quadrupole-matrix elements remain non-negligible down to threshold, one may hope to see consequences of these sign changes even without the enhancement previously discussed.

From the above discussion we see that quadrupole contributions can be important in photoelectron angular distributions for outer shells in the low-energy region, particularly when there is a significant Cooper minimum in the subshell cross section. The role of the quadrupole contribution in determining the photoelectron angular distribution can be experimentally observed through the measurement of B_1 and B_3, which to a good approximation can be characterized at these energies as a measurement of the deviation of $d\sigma/d\Omega$ from symmetry about 90°. For photoelectron energy in and below the few-keV region, B_4 and higher B_{2m} are small compared with 1; B_5 and higher B_{2m+1} are small compared with B_1 and B_3. Neglecting B_4 and all higher B_m we have

$$\frac{d\sigma}{d\Omega}=\frac{\sigma_{nLJ}}{4\pi}(\alpha+\beta)\ ,$$

where

$$\alpha=1+\frac{B_2}{2}(3\cos^2\theta-1)\ ,$$

$$\beta=B_1\cos\theta+\frac{B_3}{2}(5\cos^3\theta-3\cos\theta),$$

using the symmetry and antisymmetry of α and β under $\theta\rightarrow\pi-\theta$,

$$\frac{\beta}{\alpha}=\frac{(d\sigma/d\Omega)_\theta-(d\sigma/d\Omega)_{\pi-\theta}}{(d\sigma/d\Omega)_\theta+(d\sigma/d\Omega)_{\pi-\theta}}\ .$$

Figure 3 shows β/α as a function of θ for photoelectron energy between 0.001 and 10 keV; each panel shows a range of energies across which the energy dependence of β/α at fixed angle is monotonic. From this figure one may identify the choices of energy and angle for which the quadrupole effects are largest. Effects (+ / $-$) greater than 5% are available in several energy ranges: (+) 3$-$4 eV, ($-$) 10$-$20 eV, (+) 100$-$800 eV, and (+) above 7 keV. At low energy $B_1 \simeq B_3$ for photoeffect from s subshell,[7] as illustrated in Fig. 1. Substituting $-B_1$ for B_3 we have

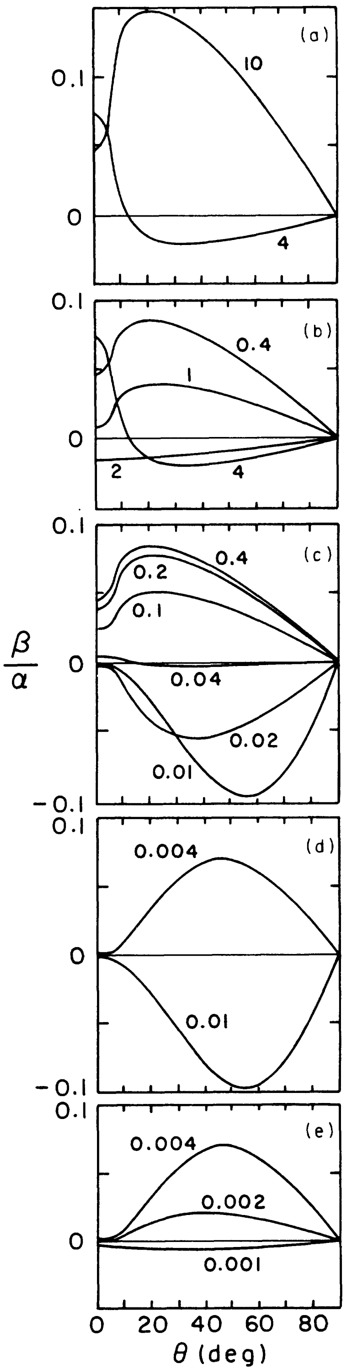

FIG. 3. The forward-backward asymmetry β/α as a function of angle (in degrees) for various photoelectron energy (a) 10 keV (top), 4 keV (bottom); (b) from top to bottom 0.4, 1, 2, and 4 keV; (c) from top to bottom 0.4, 0.2, 0.1, 0.04, 0.02, and 0.01 keV; (d) top 0.004 keV, bottom 0.01 keV; (e) from top to bottom 0.004, 0.002, and 0.001 keV.

$$\frac{d\sigma}{d\Omega} \simeq \frac{\sigma_{nLJ}}{4\pi}[(1+B_2)-\tfrac{1}{2}(3B_2-5B_1\cos\theta)\sin^2\theta] ,$$
$$\frac{\beta}{\alpha} \simeq \frac{5B_1\cos\theta\sin^2\theta}{2(1+B_2)-3B_2\sin^2\theta} . \tag{2}$$

At intermediate energies it is also a good approximation to set $B_2=-1$ as in nonrelativistic dipole approximation (well satisfied from 50 eV, above the Cooper minimum, to 10 keV), so that $\beta/\alpha \simeq \frac{5}{3}B_1\cos\theta$, giving a maximum asymmetry (0°/180°) of $\frac{5}{3}B_1$. We indeed see a trend from β/α small in the forward direction at low energy [as in Eq. (2)] to large near the forward direction at higher energy, as with $B_2=-1$.

This work was supported in part by the National Science Foundation and in part by the U.S.—Israel Binational Science Foundation (BSF), Jerusalem, Israel.

---

*Current address: Department of Physics, University of Southern California, Los Angeles, California 90007.
†Permanent address: Racah Institute of Physics, Hebrew University of Jerusalem, Jerusalem, Israel 91904.
[1]M. Ya Amusia, N. A. Cherepkov, and L. V. Chernyshena, Phys. Lett. A 40, 15 (1972).
[2]T. E. H. Walker and J. T. Waber, J. Phys. B 6, 1165 (1973); 7, 674 (1974).
[3]N. A. Cherepkov, Phys. Lett. A 66, 204 (1978).
[4]W. R. Johnson and K. T. Cheng, Phys. Rev. Lett. 40, 1167 (1978); Phys. Rev. A 20, 978 (1979).
[5]W. Ong and S. T. Manson, Phys. Rev. A 19, 688 (1979); 20, 2364 (1979).
[6]S. T. Manson and A. F. Starace, Bull. Am. Phys. Soc. 24, 1175 (1979).
[7]H. K. Tseng, R. H. Pratt, Simon Yu, and Akiva Ron, Phys. Rev. A 17, 1061 (1978).
[8]R. H. Pratt, Akiva Ron, and H. K. Tseng, Rev. Mod. Phys. 45, 273 (1973).
[9]Young Soon Kim, R. H. Pratt, Akiva Ron, and H. K. Tseng, Phys. Rev. A 22, 567 (1980).
[10]The notation $(\Lambda,\lambda,2j,l)$ used here for dipole- and quadrupole-matrix element is the same as defined in Ref. 9.
[11]The quadrupole terms are about 10^{-1} of dipole terms. Higher multipole terms are about 10^{-2} or less of dipole terms.
[12]S. T. Manson, Phys. Rev. 182, 97 (1969).